Journal of Optoelectronic and Biomedical Materials Vol. 14, No. 3, July – September 2022, p. 137 - 144

Synthesis and characterizations of phosphorus doped ZnO nanoparticles

J. El Ghoul [a,b,*], N. Abdel All [a,c]
[a] *Imam Mohammad Ibn Saud Islamic University (IMSIU), College of Sciences, Department of Physics, Riyadh 11623, Saudi Arabia*
[b] *Laboratory of Physics of Materials and Nanomaterials Applied at Environment (LaPhyMNE), Faculty of Sciences in Gabes, Gabes University, 6072 Gabes, Tunisia*
[c] *Physics Department, Assiut University, Assiut 71516, Egypt*

We reported the synthesis of phosphorus doped ZnO nanoparticles for a concentration of P ranging from 2 to 8%by a sol–gel processing technique. The structural and optical properties of these nanoparticles were characterised by different techniques. The structural study confirms the presence of hexagonal wurtzite phase with average crystallite size around 30nm. However, the optical study was shown a high absorption in the UV range and an important reflectance in the visible range. The optical band gap of P-ZnO samples were varied between 3.32 and 3.28 eV. The aim of this work is to study the effect of phosphorus doping on the structural, morphological and optical properties of ZnO nanoparticles.

(Received March 9, 2022; Accepted August 12, 2022)

Keywords: Sol-gel process, P-doped ZnO, Structural properties, Optical materials

1. Introduction

In recent years many studies on Transparent Conductive Oxides (TCOs) have brought an important interest in nanotechnology because they may have the dual properties of having good transmittance in the visible light region and high electrical conductivity [1].These characteristics depend on the nature, the number and the atomic arrangement of the metal cations in the crystalline oxide structure, the morphology of the nanomaterials and the presence of intrinsic (oxygen vacancies and interstitial metal) or extrinsic (doping) defects. Currently, the dominant TCOs are SnO_2, TiO_2, ZnO and Indium Tin Oxide (ITO). Zinc oxide is considered today as the promising key for several nanotechnology applications. In particular, it offers good prospects as a transparent conductive oxide when doped with several types of dopants such as ytterbium (Yb), indium (In), vanadium (V) and molybdenum (Mo) [2-5]. ZnO nanostructures with different morphologies have particular properties, so there are very intense interests have been devoted to the synthesis of ZnO with various morphologies such as nanowires, nanorods and nanobelts. In fact, ZnO as a semiconductor has a wide band gap (3.3 eV), a large exciton binding energy of 60 meV at room temperature (RT) [6-7], abundant in nature and environmentally friendly; these characteristics make this material attractive for many applications such as solar cells, optical coatings, photocatalysts, antibacterial activities, electrical devices, active medium in UV semiconductor lasers and in gas sensors, thereby allowing faster detection and response [8-13]. ZnO nanomaterials can be doped with transition metals (Co, Fe, Mn, Ni, etc.) [14-17] or with poor metals (Al, Ga, In, Sn, etc.) [18-21], synthesised by several techniques (PLD, sputtering) and chemical techniques (spin-coating, pyrolysis spray, sol-gel, etc.).

* Corresponding author: ghoultn@yahoo.fr
https://doi.org/10.15251/JOBM.2022.143.137

Therefore, in this work, we describe our approach for synthesis ZnO nanoparticles and study of the influence of phosphorus doping with different concentrations on the structural, morphological and optical properties of ZnO nanoparticles.

2. Experimental details

2.1. Sample preparation

P-doped ZnO nanoparticles with various concentration of Phosphorus were prepared by a sol-gel method as follow:16 g of zinc acetate dehydrate [$ZnC_4H_6O_4.2H_2O$] (Sigma Aldrich≥99% purity) as a host precursor was dissolved in a 112 ml methanol (CH_3OH) as solvent. After 10 min of magnetic stirring at room temperature, ammonium dihydrogen phosphate ($NH_4H_2(PO_4)_2$, ≥98%) was added as the phosphorus dopant precursor with different concentrations ranging from 0 to 5%, and continue with magnetic stirring until the total dissolution of the precursors. After, the resultant solution was placed in an autoclave by adding a 220 ml ethanol (C_2H_5OH) for drying in the supercritical conditions of the latter, using the J. El Ghoul et al. protocol [22].

2.2. Characterisation techniques

The effect of phosphorus concentrations on the crystalline phase of the obtained nanoparticles was monitored with the help of Bruker D5005 powder X-ray diffractometer using CuKα (λ=1.5418 Å). There corded X-ray diffraction patterns of P-ZO were investigated in an angle (2θ) ranging from 20° to 70° with a step of 0.02°. The synthesised samples were also characterised by using a transmission electron microscope (TEM) (JEM-200 CX). The optical-absorption spectra and diffuse reflectance spectra were measured on Shimadzu (UV-3101 PC UV-Vis-NIR) spectrophotometer in the wavelength range of 200-1800 nm. The powder of $BaSO_4$ was used as a standard for the optical measurements.

3. Results and discussion

X-ray diffraction analysis was carried out to study the crystal phases of P-ZnO nanoparticles. Fig.**1** shows the XRD patterns of P-ZnO nanoparticles with different phosphorus doping concentrations. The results indicate the formation of hexagonal wurtzite phase of ZnO [23], matched well with space group $P6_3mc$ (No. 186) (JCPDS No. 36-1451). It is clear in fig.1 that, XRD patterns of different doping concentrations are similar to XRD pattern of undoped ZnO. The values of lattice constants at room-temperature of doped P-ZnO materials are agreed with hexagonal polycrystalline wurtzite structure of ZnO (a = 3.249 Å and c = 5.206 Å) [24].

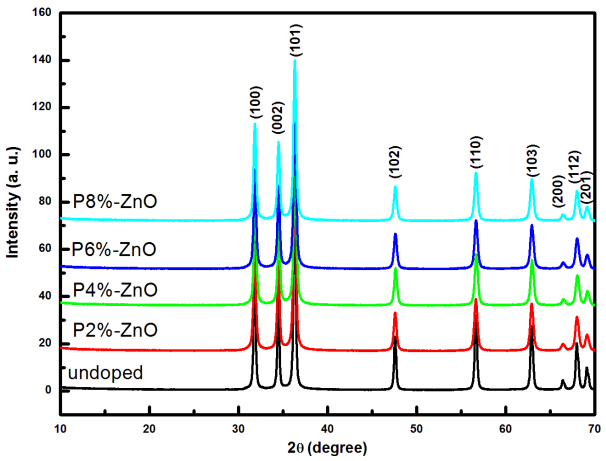

Fig. 1. X-ray diffraction patterns of undoped and P-doped ZnO.

This implies that the doping of P-ZnO has retains the same crystal structure of ZnO [25]. The average crystallite size D was evaluated using the Debye-Scherrer formula as given [26]:

$$D = \frac{0.9\lambda}{B\cos\theta_B} \quad (1)$$

where λ is the X-ray wavelength (1.5418 Å), θ_B is the maximum of the Bragg diffraction peak and B is the fullwidth at half maximum (*FWHM)* of diffracted peaks measured in radians. The crystallite size of P-ZnO nanoparticles with different doping concentrations have been calculated and summarised in Table1. The size of P-ZnO nanoparticles crystallites varies between 22 and 40 nm.

The morphology and the size of the P-doped ZnO powders have been investigated by TEM analysis (Fig. 2). As regards the particles morphology, the grains appear to become more elongated and loss their regular facets with increasing phosphorus content. However, HRTEM image of $P_{4\%}$-ZnO depicted that also in the P doped samples the grains crystallinity is still preserved.

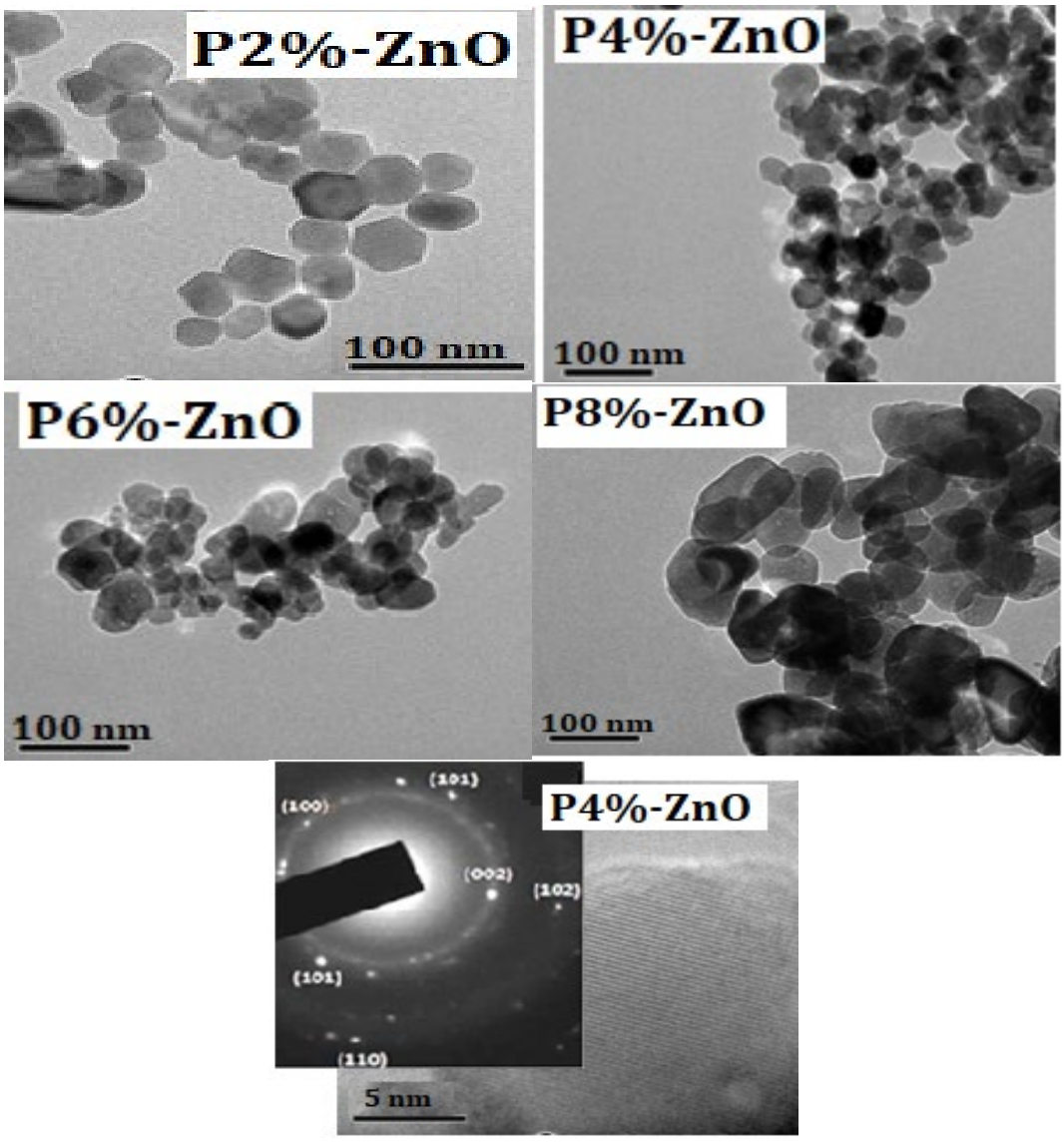

Fig. 2. TEM and HRTEM images and SAED pattern of $P_{4\%}$-ZnO.

The SAED pattern of $P_{4\%}$-ZnO clearly showed randomly scattered diffraction spots along with ring patterns, which reveal that pure as well as phosphorus doped ZnO nano-powders consist of single as well as poly-crystalline nanocrystallites. The observed diffraction spots and rings are indexed with the help of bulk ZnO JCPDS card36-1451 data.

In order to investigate the optical properties and band gap, the absorbance spectra of the samples was carried out by UV–Vis spectrophotometer. The absorbance and reflectance spectra of P-ZO nanoparticles at different concentrations of phosphorus in UV and visible range are presented in Fig.3 and Fig.4, respectively.

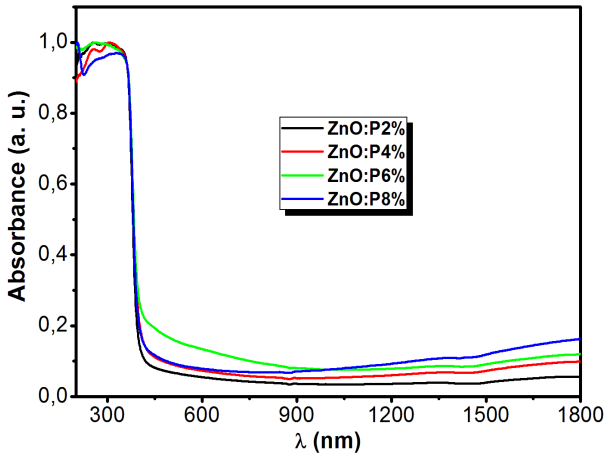

Fig. 3. UV-Vis-NIR absorbance spectra of P-ZnO nanoparticles.

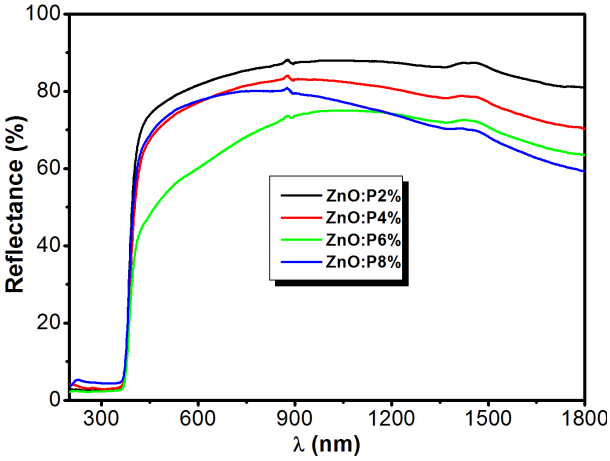

Fig. 4. UV-Vis-NIR reflectance spectra of P-ZnO nanoparticles.

It is clear that, the reflectance is varied at different doping concentrations in the UV range, which shows that absorption is the highest in this region. In contrast, the reflectance is varied between 65% and 80% in the visible light region, which prove that the optical diffusion power of this type of material is quite important in this range.

The absorption coefficient α is related to the optical energy band gap Eg for high photon energies as [27]:

$$\alpha(h\nu) = C\left(h\nu - E_g\right)^{\frac{1}{2}} \tag{2}$$

where C is a constant for direct transition, and hν is the energy of the incident photon. The plot of $(\alpha h\nu)^2$ against (hν) shows a linear dependence. This means that ZnO are direct transition type semiconductor. The band gap energy (Eg) is determined by extrapolating the linear part of the spectrum $(\alpha h\nu)^2$ curve towards the (hν) axis in Fig.5.

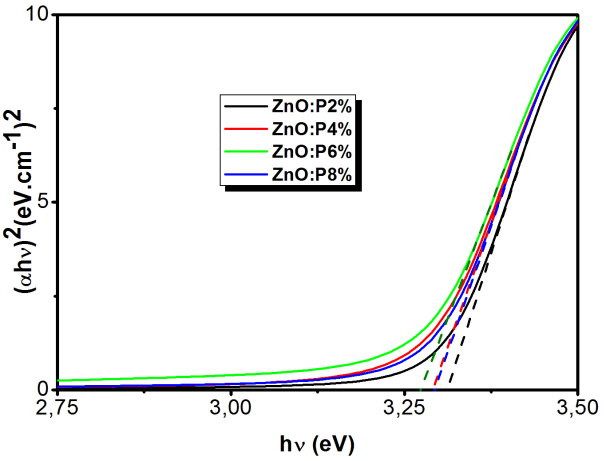

Fig. 5. Plot of $(\alpha h\nu)^2$ against (hν) of P-ZnO *nanoparticles.*

The band gap energies have been also estimated by using the method of the first derivative of the reflectance *(dR/dλ)* [28, 29]. The variation spectrum of the first derivative of the reflectance *(dR/dλ)* versus wavelength (λ) for P-ZnO nanoparticles is shown inset in Fig.6.

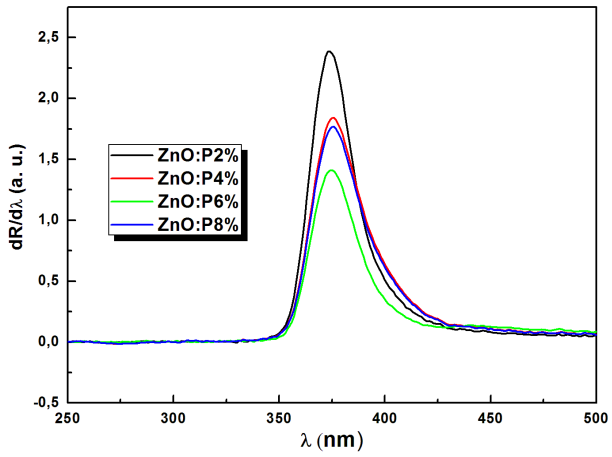

Fig. 5. Plot of first derivative reflectance of P-ZnO nanoparticles.

We found that, the estimated values of the band gap energy from this method are summarised in Table 1.

Table 1. Lattice parameters values the crystallites size and band gap energies of the samples.

P(at. %)	a (101)	c (002)	D (nm)	Eg (eV)Tauc plot	Eg (eV)First derivative
2	3.251	5.208	23	3.31	3.315
4	3.250	5.205	24	3.29	3.31
6	3.251	5.208	41	3.29	3.30
8	3.242	5.194	38	3.27	3.285

The decreases in the gap energy can be attributed to create of donor level below the conduction band or the fact that the phosphorus atoms are not completely absorbed by the host matrix of ZnO. So, some phosphorus atoms are positioned on the surface of the ZnO, giving rise to allowed states near the conduction band in the band gap. Similar results have been reported for In, Sn and Al-doped ZnO [30-32], where the oxides In2O3, SnO_2 and Al_2O_3 appear on the surfaces of the doped ZnO.

4. Conclusion

In summary, P-ZO were synthesised by a sol-gel technique. The structural study of XRD indicated that the synthesised P-ZO nanoparticles are crystallised in a hexagonal wurtzite structure with crystallite size varies between 22 and 40 nm. According to TEM analysis, the shape of crystallites was transformed from a hexagonal to spherical with increasing in its size as phosphorus concentration increased. The optical study reveals the presence of the intense absorption in the UV range as well as the significant reflectance in the visible and infrared region where these results are agreed with the common behaviour of ZnO nanoparticles. The band gap energies were estimated from the variation of two methods and their values are between 3.31and 3.27eV.

Acknowledgements

This research was supported by the Deanship of Scientific Research, Imam Mohammad Ibn Saud Islamic University, Saudi Arabia, Grant No. (20-13-12-024).

References

[1] K. Mahmood, S.B. Park, H.J. Sung, J. Mater. Chem. C. 1 (2013) 3138-3149. https://doi.org/10.1039/C3TC00082F

[2] G.H. Mhlongo, B.M. Mothudi, K.T. Hillie, and M.S. Dhlamini, Mater. Lett.119 (2015) 71-74. https://doi.org/10.1016/j.matlet.2013.12.076

[3] J. El Ghoul, J. Mater. Sci: Mater Electron 27 (2015) 1-7 https://doi.org/10.1007/s10854-015-4006-z

[4] G. Chen, X. Zhao, H. Zhang, F. Liu, Y. Wang, H. Wang, J. Gao, Y. Zhao, W. Li and J. Tao, Superlattices Microstruct 99 (2016) 175-181. https://doi.org/10.1016/j.spmi.2016.03.017

[5] C. Manoharan, G. Pavithra, S. Dhanapandian and P. Dhamodharan, Spectrochim. Acta, Part A 149 (2015) 1-22. https://doi.org/10.1016/j.saa.2015.04.024

[6] J. El Ghoul, Bull. Mater. Sci 39 (2016) 7-12. https://doi.org/10.1007/s12034-015-1139-x

[7] L. Yan, C.K. Ong and X.S. Rao, J. Appl. Phys 96 (2004) 508-511. https://doi.org/10.1063/1.1757652

[8] P. Sharma, K. Sreenivas and K.V. Rao, J. Appl. Phys 93 (2003) 3963-3970.

https://doi.org/10.1063/1.1558994
[9] Ü. Özgür and H. Morkoç, Zinc Oxide Bulk, (1st Edition) (Elsevier, Thin Films. Nanostruct, (2006) 1-600.
[10] T. Movlarooy and J. Magn. Magn. Mater 441 (2017) 139-148.
https://doi.org/10.1016/j.jmmm.2017.05.055
[11] R. Razali, A. Khorsand Zak, W.H.A. Majid and M. Darroudi, Ceram. Int 37 (2011) 3657-3663.
https://doi.org/10.1016/j.ceramint.2011.06.026
[12] C.L. Hsu,D.X. Hsu,T.J. Hsueh,S.P. ChangandS.J. Chang, Ceram. Int 43 (2017) 5434-5440.
https://doi.org/10.1016/j.ceramint.2017.01.035
[13] Y. Dou, F. Wu, C. Mao, L. Fang, S. Guo and M. Zhou, J. Alloys Compd 633 (2015) 408-414.
https://doi.org/10.1016/j.jallcom.2015.02.039
[14] J. El Ghoul, M. Kraini and L. El Mir, J Mater Sci: Mater Electron 26 (2015) 2555-2562.
https://doi.org/10.1007/s10854-015-2722-z
[15] J. El Ghoul, M. Kraini and O.M. Lemine, J Mater Sci: Mater Electron 26 (2015) 2614-2621.
https://doi.org/10.1007/s10854-015-2732-x
[16] L. El Mir, Z. Ben Ayadi, H. Rahmouni, J. El Ghoul, K. Djessas and H.J. von Bardeleben, Thin Solid Films 517 (2009) 6007-6011.
https://doi.org/10.1016/j.tsf.2009.03.197
[17] J. El Ghoul, Bull. Mater. Sci., 39 (2016) 7-12.
https://doi.org/10.1007/s12034-015-1139-x
[18] M. Hjiri, R. Dhahri, K. Omri, L. El Mir, S.G. Leonardi, N. Donato and G. Neri, Mater. Sci. Semicond. Process 27 (2014) 319-325.
https://doi.org/10.1016/j.mssp.2014.07.009
[19] S. Ameen, M.S. Akhtar, H.K. Seo, Y.S. Kim and H.S. Shin, Chem. Eng. J 187 (2012) 351-356.
https://doi.org/10.1016/j.cej.2012.01.097
[20] I. Ghiloufi, J. El Ghoul, A. Modwi and L. El Mir, Mater. Sci. Semicond. Process 42 (2016) 102-106.
https://doi.org/10.1016/j.mssp.2015.08.047
[21] M. Hjiri, L. El Mir, S.G. Leonardi, A. Pistone, L. Mavilia and G. Neri, Sens. Actuators, B 196 (2014) 413-420.
https://doi.org/10.1016/j.snb.2014.01.068
[22] J. El Ghoul J Mater Sci: Mater Electron 27 (2016) 2159-2165.
https://doi.org/10.1007/s10854-015-4006-z
[23] J. El Ghoul, C. Barthou, M. Saadoun and L. El Mir, J. Phys. B 405 (2010) 597-601.
https://doi.org/10.1016/j.physb.2009.09.072
[24] J. El Ghoul, C. Barthou and L. El Mir, SuperlatticesMicrostruct. 51 (2012)942-951.
https://doi.org/10.1016/j.spmi.2012.03.013
[25] C.S. Prajapati and P.P. Sahay, Mater. Sci. Semicond. Process 16 (2013) 200-210.
https://doi.org/10.1016/j.mssp.2012.04.015
[26] J. El Ghoul, N. Bouguila, S.A. Gómez-Lopera and L. El Mir, Superlattices Microstruct 64 (2013) 451-459.
https://doi.org/10.1016/j.spmi.2013.10.018
[27] R. Slama, J. El Ghoul, K. Omri, A. Houas, L. El Mir and F. Launay, J Mater Sci: Mater Electron 27 (2016) 7939-7946.
https://doi.org/10.1007/s10854-016-4786-9
[28] G. Riveros, H Gomez, R. Henríquez, R. Sshrebler, R. Cordova, R.E. Marotti and E.A. Dalchiele, Soc. Chil. Quim. 47 (2002) 1-17.
https://doi.org/10.4067/S0366-16442002000400013
[29] G. Kaur, A. Mitra and K.L. Yadav, Progress in Natural Science: Mater Inter 25, (2015)12-21.
https://doi.org/10.1016/j.pnsc.2015.01.012
[30] S. Alamdari, M.J. Tafreshiand, M.S. Ghamsari, Mater. Lett 197 (2017) 94-97.
https://doi.org/10.1016/j.matlet.2017.03.113

[31] R. Henríquez, P. Grez, E. Muñoz, H. Gómez, J.A. Badán, R.E. Marotti and E.A. Dalchiele, Thin Solid Films 518 (2010) 1774-1778.
https://doi.org/10.1016/j.tsf.2009.09.030
[32] C. Wu, L. Shen, H. Yu, Q. Huang and Y.C. Zhang, Mater. Res. Bull.46 (2011) 1107-1112.
https://doi.org/10.1016/j.materresbull.2011.02.043